buildings

MDPI

Article

The Interface Transition Region (ITR) in 3D Printed Concrete: A Mechanistic Taxonomy and Constitutive Requirements for Interlayer Stress Transfer

Oleg V. Kabantsev [1], David Cajamarca-Zuniga [1,*] and Aleksey V. Karlin [2]

[1] Directorate for Scientific and Technical Projects, National Research University Moscow State University of Civil Engineering, Moscow 129337, Russia; KabantsevOV@mgsu.ru
[2] Center for Specialized Projects, National Research University Moscow State University of Civil Engineering, Moscow 129337, Russia; KarlinAV@gic.mgsu.ru
* Correspondence: KakhamarkaSS@mgsu.ru or ccajamarcaz@ucacue.edu.ec

Abstract

3D concrete printing (3DCP) creates interlayer interfaces that often govern structural performance under tensile and shear loading. Despite extensive research on manufacturing parameters, the field lacks a unified framework for interfacial stress transfer, and terms such as bond, adhesion, cohesion, and interlocking are used inconsistently. This paper addresses that gap in three steps. First, it distinguishes the interface, an idealised zero-thickness boundary, from the finite-thickness Interface Transition Region (ITR) formed where two cementitious surfaces of the same material meet with different physicochemical histories at deposition. Second, it proposes a taxonomy of four interacting stress-transfer mechanisms (adhesion, cohesion, friction, and interlocking). Third, the taxonomy is confronted with an orthotropic constitutive model for 3DCP concrete, interpreted as an adhesion-dominated limit case under tensile stress perpendicular to the printing layers; coupled normal–tangential transfer reported for an analogous discrete interface; and six constitutive formulations, evaluated for the mechanisms each represents or neglects. The synthesis yields five physically grounded requirements for future constitutive treatments of these interfaces.

Keywords: interlayer bonding; adhesion–cohesion–friction; interface; anisotropic concrete; interlocking

1. Introduction

Extrusion-based 3D concrete printing (3DCP) has moved, over the past decade, from a laboratory curiosity to a technology actively pursued for structural-scale construction, driven by its potential to reduce formwork requirements, labour intensity, and construction time relative to conventional cast-in-place methods [1]. The technology fabricates elements by depositing cementitious material as successive extruded layers without the compaction step inherent to conventionally cast concrete. This manufacturing process produces a layered, piecewise-homogeneous material structure with a markedly anisotropic mechanical response, in which the behaviour of the interfaces between successive layers plays a substantial role, as demonstrated by systematic mechanical characterisation of 3DCP [2].

Over the past fifteen years, the overall volume of scientific literature within the broader field of 3DCP has increased markedly, as evidenced by the historical evolution of diverse document types published since 2010 (Figure 1a, adapted from [3], which provides aggregate bibliometric context for the whole field). As the discipline moves towards rigorous

Check for updates

Academic Editor: Antonio Caggiano

Received: 27 September 2026
Revised: 18 October 2026
Accepted: 26 October 2026
Published: 30 October 2026

Copyright: © 2026 by the authors. Licensee MDPI, Basel, Switzerland. This article is an open access article distributed under the terms and conditions of the Creative Commons Attribution (CC BY) license.

structural validation, research attention has increasingly turned towards the physics of interlayer behaviour. In this study, a targeted, mechanism-oriented literature search was conducted to identify and examine publications addressing the underlying stress-transfer mechanisms across the extruded layers (Section Literature Search Strategy and Scope). The 52 records screened (Figure 1b) are a purposive selection, not a sample of the field; their annual distribution describes the composition of this screened set only. Because the two panels differ in population, period and document types, they are not directly comparable, and Figure 1b is not offered as evidence of field-wide trends.

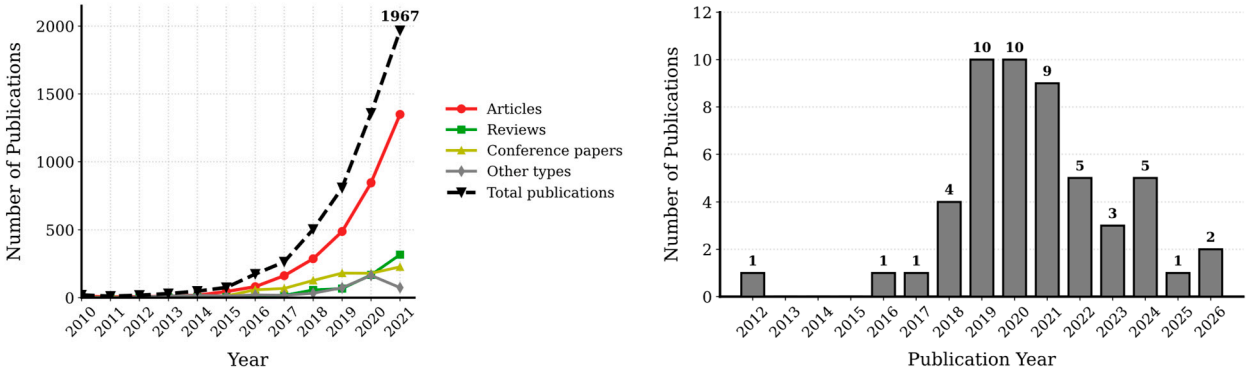


Figure 1. Bibliometric context and composition of the screened literature. (**a**) Annual scientific production in extrusion-based 3D concrete printing (3DCP) by document type, 2010–2021 (adapted from [3]); this panel characterises the broader field. (**b**) Annual distribution (2012–2026) of the 52 records screened in the present study (Section Literature Search Strategy and Scope), compiled by the authors; this panel describes the composition of a purposive set only. The two panels differ in population, period and document types and are not directly comparable; neither supports inferences about field-wide trends in interlayer research.

A substantial body of experimental research has responded to this obstacle by characterising interlayer bond strength as a function of manufacturing parameters, most extensively the time interval between the deposition of successive layers [2,4–8], but also nozzle standoff distance, printing speed, substrate moisture, and mixture composition [9–12]. Two recent review efforts have begun to synthesise this body of work: a systematic review of testing methods and reported improvement strategies [13], and a critical review comparing existing analytical and numerical models for interlayer microstructure and mechanical properties [14]. Both reviews, together with the broader state-of-the-art synthesis [15] and a component-scale review connecting interlayer bond strength, anisotropy, and process parameters to the axial performance of printed walls [16], confirm that the field possesses substantial empirical knowledge of *which* process variables affect interlayer strength, and a growing, but still fragmented, set of individual constitutive and analytical proposals addressing specific aspects of *how* that strength is generated or lost.

What remains absent, according to the reviewed literature, is a conceptual framework capable of organising this knowledge around an explicit answer to a more fundamental question: through which physically distinguishable mechanisms is stress actually transferred across a 3DCP interlayer interface, and how does the manufacturing process govern the relative contribution of each? In the absence of such a framework, terms such as *bond*, *adhesion*, *cohesion*, and *interlocking* are used across the literature in ways that are individually clear within a given study but not consistently distinguished across studies. As a result of this terminological and conceptual gap, interlayer performance continues to be reported predominantly as a single scalar outcome (a bond strength) obtained from a test method (splitting, direct tension, shear) that typically convolves more than one mechanism without

isolating any of them explicitly, so that the stress-transfer process itself is rarely analysed explicitly. This terminological and conceptual fragmentation is not merely a matter of vocabulary. The constitutive and analytical formulations for 3DCP interlayer interfaces surveyed in the present work achieve internal consistency by explicitly representing between one and three mechanisms, while implicitly absorbing the remainder into an already-calibrated parameter. This practice is defensible within the narrow scope for which each formulation was developed, but it precludes the physical interpretation of that parameter outside that scope and the direct comparison or integration of formulations.

The present paper addresses this gap by introducing a conceptual distinction between the interlayer interface, treated as an idealised zero-thickness mechanical boundary in the manner standard to cohesive-zone and traction-separation formulations, and the "*Interface Transition Region*" (ITR), which is the finite-thickness material region generated by the contact between cementitious surfaces of the same material system but with different physicochemical histories at the instant of the layer deposition. This distinction is deliberately drawn apart from the classical Interfacial Transition Zone (ITZ) of conventional concrete technology, which arises from compositional rather than temporal heterogeneity. Based on this distinction, the paper proposes a taxonomy of four interacting stress-transfer mechanisms (adhesion, cohesion, friction, and mechanical interlocking), clarifying in particular that mechanical interlocking, when produced deliberately through grooved or ribbed nozzle geometries, is a mechanism whose physical origin lies within the finite-thickness ITR and which requires explicit homogenisation before it can be represented at the idealised interface. The proposed framework is then used to reorganise a substantial portion of the existing experimental literature according to which of these four mechanisms it is best interpreted as probing, rather than according to the process variable it manipulates, and to propose an explicit process-variable-to-mechanism mapping. The resulting taxonomy is compared with constitutive evidence: the orthotropic model for 3DCP concrete [3], representing an adhesion-dominated limit case under tension perpendicular to the printing layers (tensile stress normal to interfaces); experimental evidence of coupled normal–tangential stress transfer obtained in an analogous discrete cementitious interface (brick–mortar masonry [17]), invoked as methodological precedent; and a structured comparison against six identified constitutive and analytical formulations for 3DCP interfaces. This synthesis is translated into five explicit, falsifiable requirements that a future constitutive treatment of 3DCP interlayer interfaces should satisfy.

Consistent with the scope defined above, this paper is a conceptual and synthesis-based contribution. It is not an experimental study, since it reports no new experimental data, and it is not intended as a comprehensive review, since the literature was selected to test a mechanism-oriented framework (Section Literature Search Strategy and Scope) and extensive coverage of the field is already provided by recent reviews. It does not propose a calibrated constitutive law; this, and its experimental validation, are deliberately deferred to subsequent stages of a broader research programme, for which the requirements of Section 6 are intended to provide an explicit and checkable specification. The contribution should accordingly be assessed as a conceptual and terminological framework applied as an analytical lens to published evidence.

Literature Search Strategy and Scope

The mechanical behaviour of the interlayer interface in extrusion-based 3DCP has already been the subject of at least four substantial reviews: a concise review [13] (61 references), a critical review of interlayer microstructure and mechanics [14] (100 references), a broader material-perspective review [15] (211 references), and a recent component-scale review connecting interlayer bond strength, anisotropy, and process parameters to the axial

performance of printed walls [16] (114 references). So, the literature underlying this paper was assembled through a targeted, mechanism-oriented search rather than a systematic review, since the objective of the present work is the conceptual reorganisation of an already well-mapped field rather than exhaustive coverage; extensive coverage of the field has already been provided by these four recent literature reviews [13–16]. Records were identified in the Scopus and Web of Science databases using combinations of keywords from three concept groups: (a) extrusion-based 3D concrete printing; (b) interlayer, interface, bond, adhesion, cohesion, friction or interlocking; and (c) strength, deposition time interval, moisture, porosity, constitutive or analytical modelling. The search covered the last 15 years and targeted peer-reviewed journal articles; however, some conference papers and book chapters were added due to their quantitative interlayer data. Google Scholar was used as a supplementary source. The search returned 52 unique records. These were screened by title, abstract and, where necessary, full text against the following inclusion criteria: (i) the source reports experimental, analytical, or numerical evidence directly bearing on the mechanical behaviour of the interlayer interface in extrusion-based 3DCP (or shot-based 3DCP where explicitly noted as a comparative case); (ii) the source reports a quantifiable relationship between a manufacturing/process parameter and a measurable mechanical or microstructural outcome, or proposes a constitutive/analytical formulation for the interface; and (iii), for the discrete-interface analogy, the source provides directly comparable cohesive-frictional interface characterisation obtained by full-field experimental-numerical methods. Records not meeting criteria (i)–(iii) were excluded. A final corpus of 38 sources was retained; it corresponds to the numbered references [1–38], so that the corpus is fully identified. It comprises sources retained from this screening together with sources from analogous systems (masonry, the conventional-concrete ITZ, and continuum-mechanics background) identified separately for the conceptual framework. The 38 sources, with their type, evidence domain and the mechanism assigned to each, are listed in Table A1 (Appendix A). The search was purposive, not systematic. It is not claimed to be exhaustive or reproducible in the PRISMA sense, and it does not establish that the selection represents the whole state of the art; the conclusions of this paper are accordingly restricted to the corpus examined.

2. Conceptual Framework

2.1. The Interface as an Idealised Mechanical Boundary

Within the framework of continuum mechanics, an interface is classically treated as a surface of negligible thickness across which tractions are transmitted, and relative displacements may develop between two adjacent material domains [18]. This idealisation underlies virtually every cohesive-zone and traction-separation formulation used in computational mechanics, including those already applied to 3D printed concrete interfaces [19,20] and to discrete masonry interfaces [17]. Its value lies in tractability: a zero-thickness surface can be assigned a traction-separation law relating interface tractions t_n, t_s, t_t to relative displacements $\delta_n, \delta_s, \delta_t$, without requiring the finite-thickness material region to be resolved explicitly in a structural-scale model.

The idealisation, however, is a modelling choice, not a physical claim. It presupposes that whatever physical processes generate the interface's mechanical response can be adequately concentrated onto a surface, an assumption that is reasonable when the physical transition region is thin relative to the structural elements of interest, but which requires explicit justification when the transition region has a finite, manufacturing-controlled geometry, as in the case for extrusion-based 3DCP.

2.2. The Interface Transition Region (ITR)

Unlike conventionally cast concrete, where the fresh mixture is placed and consolidated as a single continuous body, extrusion-based 3DCP builds structural elements by successive deposition of layers, each printed onto a substrate of the same material that has already undergone a finite period of rheological evolution, moisture redistribution, and hydration [2,4,21]. At the instant a new layer is deposited, its lower surface is nearly fresh, while the upper surface of the previously printed layer has already stiffened, lost moisture, and begun to hydrate. The two surfaces brought into contact therefore belong to the same material system, yet possess markedly different physicochemical states.

We refer to the material region generated by the interaction between these two surfaces as the *Interface Transition Region (*ITR*)*: the finite-thickness region whose microstructure, porosity, degree of hydration, moisture state, and mechanical continuity may differ from those of the adjacent portions of the printed layers and may continue to evolve after deposition, and which physically mediates every stress-transfer mechanism discussed in Section 3.

The ITR is deliberately distinguished from the classical Interfacial Transition Zone (ITZ) of conventional concrete technology, which develops between the cement paste and embedded constituents of different composition, such as coarse aggregate or fibres [22,23]. The ITZ is a consequence of compositional heterogeneity within an otherwise monolithic casting process. In contrast, the ITR is associated primarily with the temporal discontinuity in an otherwise compositionally homogeneous material: the same mix is deposited twice, at two different physicochemical states, separated by the interval elapsed between the deposition of consecutive layers under the action of determined environmental conditions. The two concepts are therefore not interchangeable, and the present work does not propose the ITR as a replacement for the ITZ, but as a conceptual region-scale framework for interpreting interlayer behaviour in extrusion-based additive manufacturing.

The ITR should therefore be understood as a modelling concept supported by physical reasoning and by observations reported in the literature; it organises and gives a name to a region whose existence is already implicit throughout the experimental literature (surface moisture measurements, interlayer porosity characterisation, SEM imaging of the contact zone [24–26]), rather than as a claim that this region possesses a uniquely defined, fixed geometry or thickness. The thickness and internal structure of the ITR are expected to depend on the deposition interval, mixture rheology, moisture exchange, hydration state, and the manufacturing parameters governing layer geometry, and are not assumed constant across studies or mixtures.

In relation to concepts already in use, the ITR differs from the idealised zero-thickness interface, which is a modelling abstraction without physical extent, and from the classical ITZ, which arises from compositional heterogeneity between paste and embedded constituents. The ITR instead refers to a finite region within a single material system, whose state is generated by a process-controlled deposition interval. The contribution claimed is a conceptual framing that links process variables, interface state and constitutive representation; it is not a new measurement method.

Operational Identification of the ITR

To make the concept testable, the ITR is identified, for a given specimen and age, as the region on both sides of the nominal contact plane within which a measurable property (for example, porosity, local elastic modulus, or anhydrous cement content) departs from its value in the adjacent layer interior by more than a tolerance fixed a priori and reported, measured along profiles normal to the interface. Its thickness is then the distance over which this departure persists. It is consequently a property-specific and age-specific quantity:

values obtained from different properties need not coincide, and no single thickness is implied. Techniques already employed in the reviewed literature for this purpose include micro-computed tomography of interlayer porosity, nano-indentation of the hydration-product structure, mercury intrusion porosimetry on specimens extracted from bulk and interfacial regions, and SEM imaging of the contact zone. No ITR thickness is proposed here; its value must be established experimentally for each mixture, deposition interval and environmental condition. However, as an order of magnitude only, [3] reports that, in each printed layer, the outer part, up to approximately 20% of the layer volume (region 2 in Figure 2b), is more porous than the central part. This is a feature of the individual layer and not an ITR thickness. We emphasise that, under the operational definition above, the ITR must be established for each property, mixture, interval and age.

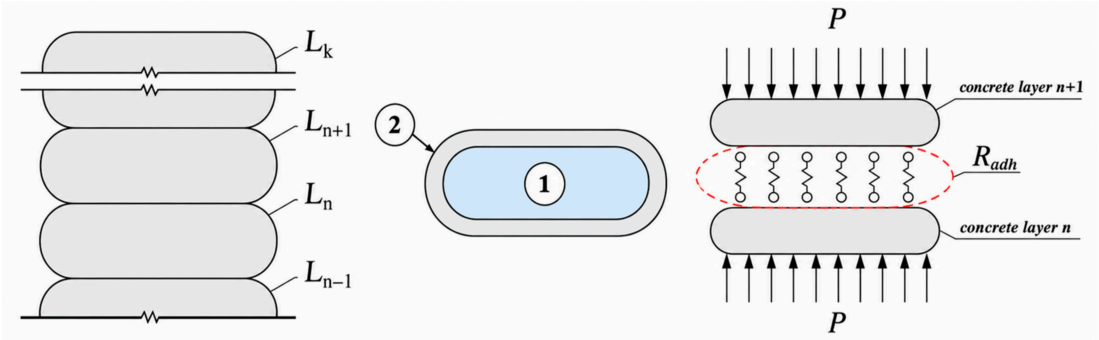


Figure 2. Schematic representation of the layer-by-layer structure and the interlayer contact zone in extrusion-based 3DCP, illustrating the physical basis of the Interface Transition Region (ITR). (**a**) scheme of the layers in the structure; (**b**) scheme of the layer structure (1—central region of the layer; 2—outer region of the layer); (**c**) scheme of the interaction between the layers in the structure.

2.3. Two Complementary Levels of Description

The distinction established above allows the mechanical behaviour of an interlayer interface to be addressed at two complementary levels, rather than as a single undifferentiated phenomenon. The physical description concerns the physicochemical processes that generate and govern the evolution of the ITR: hydration kinetics at two different degrees of advancement on either side of the contact surface, moisture exchange and evaporation from the printed filament's upper surface prior to the deposition of the next layer, rheological stiffening of the substrate, and, where the printing process employs a grooved or textured nozzle, the finite geometric relief imprinted onto the upper surface of the lower layer. The mechanical description concerns the equivalent representation adopted for structural analysis, in which the net effect of the ITR is concentrated onto the idealised interface through a constitutive relationship between interface tractions and relative displacements.

These two levels do not describe different physical objects; they are complementary levels of interpretation of the same phenomenon. The physical description explains why the interface responds as it does; the mechanical description provides the abstraction required to embed that response into a structural-scale model. A central position of the present work is that the two-level description is particularly important when the interlayer response includes mechanical interlocking. A geometric tooth or groove imprinted on the layer surface by a textured or grooved nozzle has a finite depth, pitch, and orientation [27,28]. Such geometry cannot be represented directly by a conventional zero-thickness surface without first being homogenised into an equivalent traction contribution. The required operation may be understood as a homogenisation or scale-transition step in which the finite geometry and its associated contact, separation, sliding, and possible dilation are

represented through an equivalent traction–separation response at the structural-model scale. The specific form of this equivalent response depends on the geometry, loading direction, contact conditions, and constitutive assumptions adopted. Sections 3 and 3.4 make this homogenisation step explicit rather than leaving it implicit, which we identify as one of the sources of terminological and conceptual inconsistency in the current literature.

3. A Mechanistic Taxonomy of Interlayer Stress Transfer

The overwhelming majority of the experimental literature on 3DCP interlayer behaviour reports a single scalar outcome (an interlayer bond strength, obtained from a splitting test, a direct tensile test, or a shear test) as a function of one or more manufacturing parameters: deposition time interval [2,4,5], nozzle standoff distance [9], printing speed, surface moisture at the time of deposition [10], or mixture composition [11]. This body of work has been essential in mapping which parameters matter, but a single scalar cannot, by construction, distinguish why the parameter matters: a reduction in bond strength caused by insufficient physicochemical contact is not mechanically the same event as a reduction caused by the absence of geometric interlocking, even though both may register as a lower splitting strength in an identically instrumented test.

Moelich et al. [12] anticipated part of this concern from a different angle, proposing that the relationship between surface moisture and interlayer adhesion itself passes through distinct regimes (their Stage I, where air entrapment, thixotropy, and surface roughness dominate and moisture is essentially unchanged; Stage II, where evaporation and bleeding actively control surface moisture; and Stage III, where moisture within the pore system is depleted and air penetrates the pore network), which is broadly consistent with, though narrower in scope than, the mechanism-superposition argument developed below. Their study expresses this explicitly, formulating the lack of interlayer adhesion (IA) as proportional to the surface moisture available at the instant the overlayer is placed ($IA \propto SM_f = SM_i + B_{pt} - pt\left(ER_{pt}\right)$), where SM_f [kg/m^2] is the surface moisture at placement of the overlayer, SM_i [kg/m^2] is the substrate's initial surface moisture, B_{pt} [kg/m^2] is bleeding accumulated over the pass time, pt [h] is the pass time, and ER_{pt} [kg/m^2/h] is the environmental moisture evaporation rate. Fitted against experimental data with a Root Mean Square Error (RMSE) of 2.5%, this formulation is, in our reading, the closest existing precedent among the reviewed literature for the kind of physically-traceable parameterisation that requirement R5 of the present work calls for: every term on the right-hand side corresponds to a measurable physical quantity at the ITR, rather than to a curve-fit constant against elapsed time as such.

We therefore propose that interlayer stress transfer be interpreted as the superposition of four mechanisms, each with a distinguishable physical origin, a distinguishable dependence on process parameters, and a distinguishable role over the loading history. These four mechanisms are not new to the field individually; each has been invoked, under varying terminology, by at least one strand of the literature reviewed, but they have not (to the authors' knowledge) been organised into a single explicit taxonomy applied consistently across the interlayer interface literature.

3.1. Mechanism A: Adhesion

Physical origin. Adhesion is defined here as the physicochemical bonding established between the two surfaces of the ITR during the early hydration period following deposition, prior to any mechanically significant development of bulk material strength across the contact zone. It results from the same hydration and particle-bridging processes that produce cohesion within the bulk paste, but is distinguished operationally by the fact that it

acts across the physicochemical discontinuity, between a substrate that has already partially stiffened and a fresh overlay.

The distinction between adhesion and cohesion is therefore positional and operational, not chemical: both arise from hydration and particle-bridging processes. Adhesion refers to the resistance mobilised across the contact plane while the two surfaces are still physicochemically dissimilar, whereas cohesion (Section 3.2) refers to the resistance that develops once hydration products span that plane. For this reason, the two cannot be quantified separately from a single macroscopic test. Evidence that could discriminate them includes age-dependent testing of the same interface, staged loading, and observation of the failure path (along the contact plane or into the layer interior), the latter being a diagnostic indication only.

Dependence on process parameters. Adhesion is the mechanism most directly and most severely degraded by the deposition time interval, principally moisture evaporation, rather than elapsed time as such. The full evidentiary basis for this pattern is drawn from six independent experimental studies spanning multiple mixture designs and testing methods, each reporting a specific quantitative reduction discussed in Section 4.1. Of these, Moelich et al. [12] provide the model most directly traceable to a physical state variable of the ITR rather than to a purely time-based correlation.

Mechanical signature. Because adhesion is established prior to significant bulk strength development, its mechanical signature is a comparatively low-stiffness, low-strength, and critically brittle response once its capacity is exceeded: the physicochemical bond, once broken, does not regenerate, and no significant softening branch is expected unless another mechanism (cohesion, friction, or interlocking) is simultaneously active. This is precisely the behaviour reported in [3] for 3DCP concrete loaded under tensile stress perpendicular to the printing layers, that is, normal to the interlayer interfaces (Figure 3), where the stress-strain relationship is described as closely approximated by a linear ascending branch up to a limit corresponding to the adhesive strength R_{adh}, followed by brittle failure with an unloading slope approaching zero.

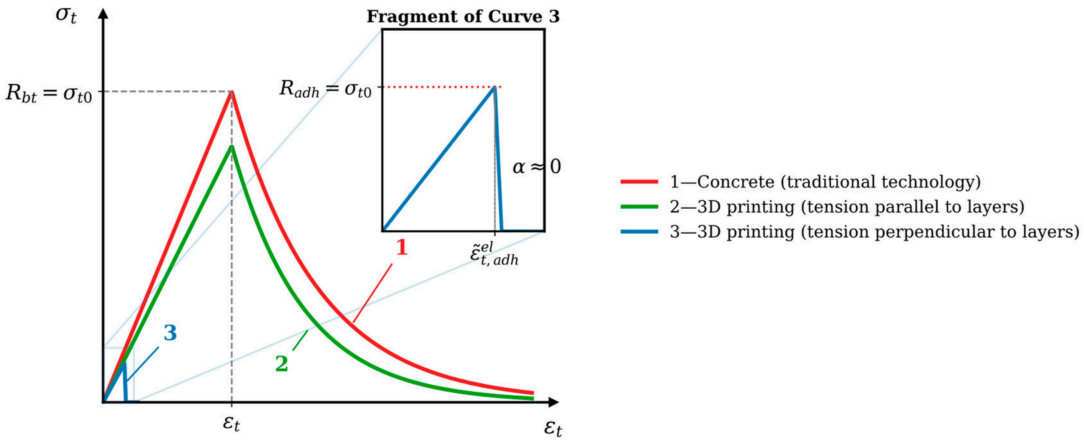


Figure 3. Stress–strain response of 3DCP concrete in tension, showing the adhesion-dominated brittle response under tensile stress perpendicular to the printing layers (curve 3) versus the cohesion-mobilised response under tensile stresses parallel to them (curve 2), relative to conventionally cast concrete (curve 1).

3.2. Mechanism B: Cohesion

Physical origin. Cohesion is defined here as the macroscopic mechanical resistance developed within the bonded cementitious material once the ITR has, at least locally, achieved sufficient continuity for stress to be transmitted through hydration products spanning the

original contact surface, rather than merely across it. Unlike adhesion, cohesion is not a property of the contact event itself but of the material that forms as a consequence of that contact continuing to hydrate. The boundary between adhesion and cohesion is operational rather than chemical, as discussed in Section 3.1.

Dependence on process parameters. Cohesion increases with curing time and is comparatively insensitive to the short-term kinetics that dominate Mechanism A, though it remains sensitive to the same porosity-generating factors discussed in Section 4.2, where the quantitative contrast between bulk and interfacial porosity reported by Rahul et al. [29] is presented in full. Geng et al. [26] proposed an explicit empirical relationship, $\sigma = K(1 - P)\sqrt{E}$, linking bond strength to interfacial porosity P and elastic modulus E. This formulation, in the present taxonomy, is best read as a constitutive expression predominantly associated with Mechanism B, since both governing variables describe the mechanical continuity of the bonded material as it develops after contact; porosity, consistent with its dual classification in Table 1, also carries a secondary dependence on the adhesive event that first established contact.

Table 1. Process-variable-to-mechanism mapping.

Process Variable	Primary Mechanism	Secondary Mechanism(s)	Key Sources
Deposition time interval/gap	A (adhesion)	B (indirectly, via porosity)	[2,4–8]
Substrate surface moisture at contact	A (adhesion)	—	[12,21]
Ambient drying/evaporation rate	A (adhesion)	—	[12,21]
Interfacial porosity/pore geometry	B (cohesion)	A (contact-area reduction)	[5,26,29] *
Bulk mix composition/w/b ratio	B (cohesion)	A (secondary, via rheology)	[26,29]
Normal compressive stress at interface	C (friction)	— (activates only post-degradation)	[17] (by analogy)
Surface roughness (non-engineered)	C (friction)	D (if geometric relief present)	[17] (by analogy)
Nozzle groove/rib geometry	D (interlocking)	C (roughness contribution)	[27,28]
Nozzle path strategy/print pattern	D (interlocking)	—	[27]
Bond-area amplification strategies	A (adhesion, area-based)	—	[36]
Deposition process (spray-based vs. extrusion)	D (interlocking, roughness-based)	A (contact area); B (air-void content)	[31]

* Porosity is measured by three distinct methods across these sources, each probing a different aspect of the pore structure: Ref. [5] used micro-computed tomography specifically to track the evolution of interlayer porosity with deposition time gap; Ref. [26] combined X-ray computed tomography (macro-scale porosity P) with nano-indentation (micro-scale elastic modulus E); Ref. [29] used mercury intrusion porosimetry on specimens extracted from bulk and interfacial regions. The row groups them by the mechanism their findings support, not by shared methodology.

Mechanical signature. Cohesion may contribute to a more extended mechanical response than that associated with an idealised adhesion-dominated failure, particularly when sufficient material continuity develops across the interlayer region. This interpretation is qualitatively consistent with Kabantsev's [3] observation that 3DCP concrete under tensile stresses parallel to the printing layers, and in compression in either direction, exhibits a stress–strain behaviour qualitatively analogous to that of conventionally cast concrete, although with differences in peak stress and corresponding strain.

In the present taxonomy, this directional difference is interpreted as indirect evidence that material continuity and cohesion-related resistance (Mechanism B) may be more substantially mobilised under tensile stresses parallel to the layers than under tensile stress perpendicular to them. However, the shape of a macroscopic stress–strain curve does not, by itself, uniquely identify the microscopic mechanisms responsible for the response. The

proposed correspondence between the observed directional behaviour and the relative mobilisation of adhesion and cohesion should therefore be regarded as a mechanistic interpretation of the available evidence rather than as a direct experimental separation of the two mechanisms.

3.3. Mechanism C: Friction

Physical origin. Friction is activated once adhesive and/or cohesive resistance has been partially or fully degraded, and depends on the normal compressive stress acting across the interface (contacting surfaces), the roughness of the contact surfaces, and the residual contact conditions after the onset of relative sliding. Unlike adhesion and cohesion, friction is not a bonding mechanism in the physicochemical or hydration-based sense; it is a contact-related resistance to relative sliding and may therefore coexist with other stress-transfer mechanisms.

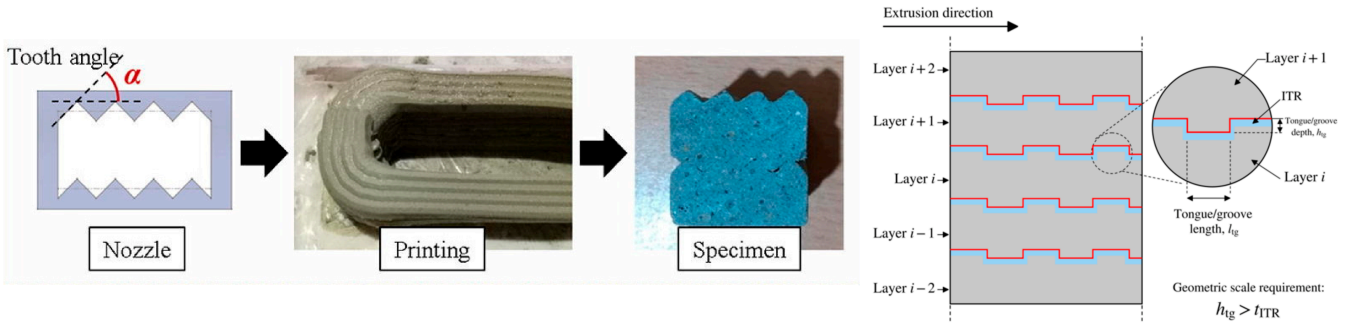
Dependence on process parameters. Friction is comparatively insensitive to the deposition time interval and instead depends on the geometric and compositional roughness of the printed surface (itself potentially influenced by process parameters such as nozzle geometry and extrusion pressure) and, critically, on the normal compressive stress present at the interface, whether externally applied or internally generated. This dependence on normal stress is what makes Mechanism C mechanically inseparable from Mechanism D in the case of grooved or textured nozzle surfaces: a Mohr–Coulomb-type formulation ($\tau_f = \tau_0 + \mu\sigma_n$) of the kind already calibrated experimentally for a discrete cementitious interface in [17] provides the natural mathematical form for Mechanism C once cohesive resistance τ_0 has been exhausted.

Mechanical signature. Friction becomes the dominant residual mechanism after substantial degradation of Mechanisms A and B, and is therefore associated with Level IV of the taxonomy proposed in Section 3.5 about residual mechanisms; it does not initiate stress transfer, but it may prevent the interface from losing all load-carrying capacity after adhesive and cohesive resistance have been consumed, provided normal compression is present.

3.4. Mechanism D: Mechanical Interlocking

Physical origin. Mechanical interlocking is defined here as the geometry-governed contribution to stress transfer arising from the physical interpenetration of material across the deposited layer boundary. In its most explicitly engineered form, this interpenetration is produced deliberately by extruding through a grooved or ribbed nozzle that imprints a longitudinal and/or transverse tooth-like relief onto the upper surface of the lower layer. When the subsequent layer is deposited, its fresh material flows into and around this relief, generating a mechanically interlocked geometry rather than a nominally flat contact surface (Figure 4).

Distinction from contact-area effects. Interlocking, as defined here, requires geometric interpenetration that resists relative displacement by changing the direction of load transfer (tooth, groove, dowel). An increase in the effective contact area between layers, for example through better wetting, fewer air voids or small-scale roughness, enlarges the area over which adhesion (A) and, under normal compression, friction (C) can act, but does not by itself constitute interlocking. Strategies acting primarily on contact area, such as the effective bond area amplification, are therefore assigned to Mechanism A (Table 1), and roughness could be assigned to Mechanism D only where the relief has a depth and orientation (like tooth, groove or dowel) capable of resisting tangential relative displacement geometrically.



(**a**) (**b**)

Figure 4. Schematic of the tooth-like interlayer interface geometry, which increases interlayer shear strength in both principal directions and illustrates the finite-thickness geometric relief that the ITR must homogenise onto the idealised interface. (**a**) Longitudinal ridge geometry formed by a grooved extrusion nozzle, restraining transverse (out-of-plane) interlayer sliding (Source: He et al. [28]); (**b**) tongue-and-groove geometry, restraining longitudinal (in-plane) interlayer sliding along the extrusion direction.

Relationship to the two-level description of the interlayer interface. Mechanical interlocking is the mechanism for which the distinction between the idealised interface and the finite-thickness ITR is not a convenience but a physical necessity. A tooth or groove has, by definition, a finite depth, pitch, and orientation; it cannot be represented directly on a zero-thickness surface. Its mechanical effect must first be homogenised (reduced to an equivalent, direction-dependent modification of the traction–separation response at the idealised interface) before it can be embedded in a structural-scale constitutive law. This is precisely the operation performed, explicitly or implicitly, by the analytical models that already exist for geometrically interlocked 3DCP interfaces. The tooth-like interface model developed by He et al. [28], expressed in terms of tooth angle and void ratio, is the clearest example: in each case, a finite-geometry effect at the ITR scale is ultimately reported as a single equivalent property (a strength ratio, an effective bond area amplification factor) at the interface scale, which is exactly the homogenisation step this taxonomy makes explicit rather than implicit.

Dependence on process parameters. Because interlocking is governed primarily by geometry rather than by the physicochemical state of the contact surfaces, its contribution is comparatively insensitive to the deposition time interval that dominates Mechanism A. This suggests a working hypothesis, not an established result. As the deposition interval increases and adhesion decreases (by approximately 50% or more at the longer intervals reported by Napolitano et al. [6], Skibicki et al. [5] and Tay et al. [7], each under its own test conditions), the relative contribution of a geometry-governed mechanism such as interlocking may increase, provided that its absolute contribution is not itself degraded. Interlocking may also depend on the interval if fresh material cannot fill the relief of a stiffened substrate. On this reading, interlocking would be the mechanism most directly available for manufacturing-level compensation for the adhesive–cohesive loss at the interface (shear strength of the interface), a proposition to be tested experimentally.

Mechanical signature. Interlocking contributes both to the initial stiffness and to the residual, post-peak load-carrying capacity of the interface, since geometric interpenetration continues to resist relative sliding after the physicochemical bond captured by Mechanisms A and B has been exhausted. In this respect, its constitutive signature overlaps partially with that of friction (Mechanism C), and the two are difficult to separate experimentally in a textured interface without dedicated testing.

Such dedicated testing is not without precedent, although not yet, to the authors' knowledge, applied to a 3DCP interlayer interface. By analogy, the work [30] proposed a

modification of the horizontal contact surface of solid clay bricks in masonry, consisting of shallow blind holes designed specifically so that mortar entering the holes during construction would contribute both frictional and geometric-interlocking resistance to the initial shear strength of the brick–mortar interface. The experimental design included a control condition in which the same holes were sealed with expanding polyurethane foam prior to bonding, preserving the surface roughness geometry while preventing mortar penetration: this isolates the geometric-interlocking contribution of the mortar-filled holes (analogous to Mechanism D) from the frictional contribution of the roughened surface alone (analogous to Mechanism C). The results showed that unsealed holes of modified solid brick (mortar-filled condition like mechanical interlocking) increased shear strength by ~45% relative to the unmodified solid brick, indicating that the geometric-interlocking contribution of the mortar dowels was substantially larger than the frictional contribution of the roughened surface by itself. However, the relative contributions of friction and interlocking were not quantified: the measured value is a total strength, and the sealing material may also alter local contact stiffness, confinement and the normal-stress distribution (sealed specimens were weaker than the unmodified brick). The study [30] is therefore cited only as an example of comparative experimental design, which suggests a strategy that could be adapted to 3DCP interlayer interfaces, not as quantitative evidence of the relative contributions of Mechanisms C and D.

A related but mechanistically ambiguous case is process-incidental roughness (surface texture arising as an unintended by-product of the deposition method itself, rather than from a deliberately engineered relief or a deliberately introduced discrete feature as shown in Figure 4). Kloft et al. [31], comparing Shotcrete 3D Printing (SC3DP) against extrusion-based deposition of an otherwise matched mix, used a barite tracer visualised by computed tomography to show that the kinetic energy of the sprayed material produces a markedly rougher interlayer contact surface than extrusion. This roughness may contribute to Mechanisms C and/or D depending on the local geometry and contact conditions, consistent with the classification of non-engineered surface roughness shown in Table 1; we do not assign it exclusively to Mechanism D.

3.5. Interaction Between Mechanisms and the Four-Level Taxonomy

The four mechanisms above are not mutually exclusive, nor do they act in a fixed order for every interface: their relative activation depends on the loading direction, the ITR's state at the time of loading (itself set by the deposition interval and curing time), and the presence or absence of engineered geometric relief (interlocking). We organise their interaction into four levels (Figure 5):

Level I: Formation mechanisms. Responsible for generating the ITR itself: hydration kinetics, moisture redistribution, and rheological stiffening prior to the deposition of the next layer, together with the imprinting of any engineered geometric relief for interlocking of the layers.

Level II: **Stress-transfer mechanisms.** Mechanisms A–D as characterised above, each engaged according to the onset conditions specified in Sections 3.1–3.4 (not necessarily simultaneously, nor from the onset of loading in every case).

Level III: Damage mechanisms. Progressive degradation of adhesive and cohesive resistance under increasing load or accumulating relative displacement, transitioning the interface's response toward the residual mechanisms below.

Level IV: Residual mechanisms. The load-carrying capacity that remains after substantial degradation of Mechanisms A and B is governed principally by friction (Mechanism C, requiring normal compression) and by any geometric interlocking (Mechanism D) still mechanically engaged.

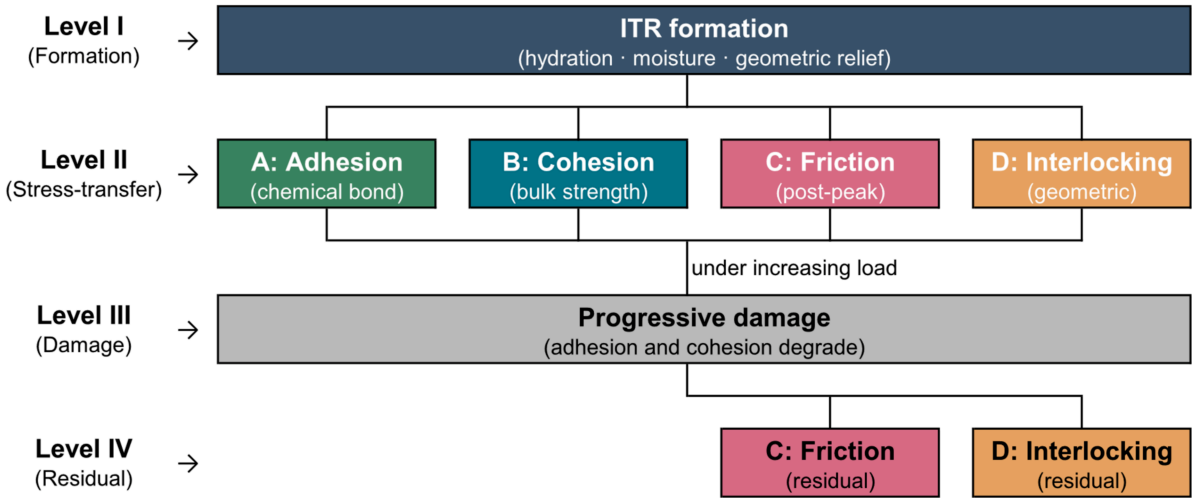


Figure 5. Proposed taxonomy of interlayer stress-transfer mechanisms (A–D) and their organisation across four interaction levels: formation, transfer, damage, and residual.

A complementary case illustrates the same ambiguity directly within 3DCP concrete. Moelich et al. [12] found that a retentive superabsorbent polymer (SAP), acting as an internal-curing agent, increased interlayer adhesion by approximately 10% by hydrating otherwise-anhydrous cement particles near the interface, whereas a self-releasing SAP of the same class decreased it. Both interventions act on a Level I formation variable (namely, the availability of water for hydration within the ITR), thereby altering the conditions under which one or more Level II mechanisms may subsequently develop. Yet the outcome variable through which Moelich et al. measure this effect, interlayer adhesion obtained by comparing printed and mould-cast specimens after full curing, is by construction an end-state comparison that cannot distinguish a deficit in initial contact quality (Mechanism A) from a failure of that contact to mature into mechanical continuity (Mechanism B). We read this not as evidence that Level I mechanisms map cleanly onto a single Level II mechanism, but as a concrete illustration of the opposite: most existing interlayer metrics, interlayer adhesion included, are composite measurements of the unresolved end-state of both mechanisms rather than of either in isolation.

A direct experimental illustration of why Levels II–IV cannot be collapsed into a single scalar bond parameter is available from studies on an analogous discrete cementitious interface [17,30]. For instance, in brick–mortar masonry joints tested under nominally pure shear (zero applied normal precompression), [17] reports normal stresses developing across the interface as tangential loading progressed to the independently measured normal adhesive strength of the studied interface. This normal-stress development, attributed to flexure of the bonded units under nominally tangential loading, is direct evidence that a shear failure event in a bonded cementitious interface is not governed by tangential resistance alone: the normal (adhesive) capacity of the interface is mobilised concurrently, even in the nominal absence of applied normal load. While this result was obtained for a discrete brick–mortar system rather than for a continuously extruded 3DCP interface, we regard it as directly relevant methodological evidence, obtained using the cohesive-interface characterisation approach, that coupling between normal and tangential stress-transfer mechanisms should be expected, and explicitly tested for, rather than assumed away, in any future constitutive treatment of 3DCP interlayer interfaces.

4. Critical Synthesis of the Literature, Organised by Mechanism

The literature on inter-layer behaviour in the 3DCP process is usually reviewed chronologically or by process parameters (time interval, nozzle geometry, mixture design) (see, e.g., [13,14]). This type of organisation is valuable for a professional seeking guidance on a specific manufacturing decision, but it tends to obscure a more fundamental question: which stress transfer mechanism, in the sense of the mechanistic taxonomy proposed for interlayer stress transfer, does a given study actually analyse? In this section, we reorganise a substantial part of the reviewed literature according to the mechanism with which it is best interpreted as being primarily associated or by which it is dominated, rather than according to the process parameter in terms of which it varies. This reorganisation is, in itself, one of the fundamental contributions that the taxonomy proposed in this paper aims to enable.

Two caveats apply throughout this section. First, the assignment of a study to a mechanism is an interpretation by the authors, based on (a) the variable manipulated and the physical quantity measured, (b) the loading configuration and failure location where reported, and (c) the explanation offered by the original authors. The assignment adopted for each source is listed in Table A1 (Appendix A). Where a study reports only a macroscopic strength, the assignment indicates the mechanism best consistent with the variable studied, not a direct experimental separation; the text distinguishes what each study measured from what is inferred here. Second, the quantitative changes cited were obtained with different mixtures, interval ranges, environmental conditions, curing regimes, test ages, loading modes, interface orientations and baselines (Table 2). It is important to note that they are reported as study-specific observations, are not pooled or ranked, and no meta-analysis is attempted; conclusions are limited to the studies examined.

4.1. Literature Dominated by Mechanism A (Adhesion)

The largest single strand of the reviewed literature from the last 15 years investigates the effect of the deposition time interval on interlayer bond strength, and is, in the interpretation adopted here, primarily probing the degradation of adhesion. Le et al. [2] provided the most cited demonstration that bond strength falls sharply as the interval between successive layers increases. Wolfs et al. [4] quantified this fall as approximately 16% (flexural) and 21% (splitting) at a 24 h interval relative to a 15 s reference, and further showed that drying exposure during the interval (rather than elapsed time alone) is the dominant driver of strength loss, with flexural strength dropping by approximately 50% between covered and uncovered specimens at an otherwise identical 4 h interval. Skibicki et al. [5] measured a 56.6% reduction in interlayer splitting strength at a 2 h gap relative to the reference condition, with the reduction stabilising near 68.5% at 4.5 h, and correlated this trend directly with an abrupt increase in interlayer porosity from 3.95% at zero gap to 9.90% at 3 h, measured by micro-computed tomography. Napolitano et al. [6] obtained a comparable order-of-magnitude reduction (approximately 50%) across a much shorter time scale (100–1800 s) using a punch-through shear configuration, and Tay et al. [7] reported a similarly steep, logarithmically decaying reduction concentrated within the first 1–10 min after deposition, with comparatively little additional loss thereafter. Subramaniam et al. [8] measured a 46% reduction in interface tensile strength (from 1.65 MPa to 0.89 MPa) between the 0-min and 9-min interfaces, using a fracture-mechanics framework.

The values quoted above refer to different mixtures, interval ranges, curing regimes, test ages and baselines (Table 2); they document the direction and order of magnitude of the effect in each study and should not be compared directly.

Table 2. Experimental conditions of the studies cited in Sections 3.4 and 4.

Ref.	Mixture (w/b)	Interval	Curing	Test Age	Loading/Orientation	*n*	Baseline
[2]	CEM I + FA + SF 70/20/10 (0.26)	0, 15, 30 min; 1, 2, 4, 8, 18 h; 1, 3, 7 d	Damp hessian + plastic, 1 d + laboratory storage	28 d	Direct tension on cored cylinders, perpendicular	6	Mould-cast cores
[4]	Weber 3D 145-2 (w/f 0.495)	15 s; 1, 4, 7, 24 h (flexural); 4, 24 h (splitting)	Plastic sheet 24 h, then water	7 d	Flexural; splitting; orientations I–III	7	15 s
[5]	OPC + FA + SF 70/20/10, sand (0.3)	1, 1.5, 2, 3, 4.5 h (splitting); 1, 2 h (flexural)	NR (printed at 20 °C; specimens cut after 48 h)	7 d	Splitting along interface; 3-p flexure; H and V compression	3	No gapprinted; cast ref.
[6]	cement mortar + PP fibres (w/c 0.38)	100, 200, 1800 s	NR	NR	Punch-through shear	4	Bulk specimens
[7]	OPC + FA + SF 70/20/10 (0.46)	1, 5, 10, 20 min	NR	NR	Direct tension, perpendicular	4	1 min
[8]	OPC 53 + PP fibres, sand/cement 1:1	0, 3, 6, 9 min	Wet burlap + laboratory environment	NR	Split tension; 3-p bending; load perpendicular to interface	3	4 s
[12]	CEM II + FA + SF (w/b 0.32)	50 s; 2, 3, 4 min	No protection, 23 °C, RH 52%	56 d	Four-point bending	6	Mould-cast same mix
[26]	PII + FA + BT + SF + PNS+ HPMC (w/b 0.38)	0.1, 3.5, 7 h; drying 0, 6, 20 min	Sealed plastic film, 20 °C	28 d	Splitting along interface	6	Ref group
[27]	60% CSA + 40% OPC (0.50)	12 min	Moulds 24 h, then water	1, 3, 7, 28 d	Compression along interface; splitting	96	Flat interface
[28]	OPC + FA + SF, 70/20/10 (0.46)	≈10 s	Plastic sheet, 25 °C	28 d	Tension; shear (3-p bending)	4/test	Flat interface
[29]	OPC + FA + SF/attapulgite/HPMC (0.32, derived)	2 min (H), 8 min (V)	NR	NR	Direct bond shear, Ø25 × 40 mm cylinders	6/test	Mould-cast cylinders
[31]	Nafufill KM 250 (0.27)	0, 15, 60, 120 min	Foil 7 d, water, 20 °C	14 d	3-p bending, H and V compression	NR	Vibrated
[36]	OPC + sand (w/c 0.36)	15 min	Ambient 23 °C	7 d	Direct tension, perpendicular	≥9	no paste

NR = not reported; Baseline = condition against which each study normalises its results; *n* = number of replicates; H/V = horizontal/vertical interface; w/b = water-to-binder ratio; w/c = water-to-cement ratio; w/f = water-to-fines ratio; CEM I = Portland cement CEM I (EN 197-1); CEM II = Portland-composite cement (EN 197-1); OPC = ordinary Portland cement; OPC 53 = ordinary Portland cement of 53-grade strength class; PII = Portland cement type II (Chinese cement classification); CSA = calcium sulfoaluminate cement; FA = fly ash; SF = silica fume; BT = bentonite; PP = polypropylene; PNS = polynaphthalene sulfonate; HPMC = hydroxypropyl methylcellulose. Weber 3D 145-2 and Nafufill KM 250 are commercial product designations.

Two studies within this strand move beyond correlating bond strength with elapsed time and instead propose an explicit physical driving variable for adhesion loss, which we regard as considerably more useful for the present taxonomy than a time-based correlation alone, since elapsed time is a proxy for (rather than a cause of) the underlying physico-chemical state of the ITR. Roussel [21] identified drying of the substrate surface as capable of halving interlayer strength independently of elapsed time per se. Moelich et al. [12] went further by developing an explicit analytical model that relates the loss of interlayer adhesion to the surface moisture available at the instant of contact (Mechanism A) and the formation of the ITR.

4.2. Literature Dominated by Mechanism B (Cohesion)

A smaller but methodologically distinct strand of the literature examines the microstructural continuity of the bonded material itself, rather than the initial contact event, and is here interpreted as probing Mechanism B. Rahul et al. [29] reported that bulk porosity in 3DCP concrete is 6–8% lower than in cast concrete, while interfacial porosity is 11–14% (horizontal interfaces) to 10–16% (vertical interfaces) higher, a contrast that, within the present taxonomy, is consistent with adhesion (Mechanism A, governed by the contact event) and cohesion (Mechanism B, governed by bulk continuity) responding to different aspects of the manufacturing process, since a well-consolidated bulk material and a poorly bonded interface are not mutually exclusive outcomes. Geng et al. [26] provided the most explicit constitutive expression of this strand, proposing an empirical relationship for interface bonding strength (σ, MPa) related to the macro and micro structure of layer interface, $\sigma = K(1 - P)\sqrt{E}$, linking interlayer strength to interfacial porosity P and elastic modulus E of "contacting areas", where K is the slope of the fitted line, of which the value is approximately 5.26×10^{-4} GPa$^{0.5}$. This expression was derived from a dual-hierarchical structural model combining macro-scale interface roughness/deformation with micro-scale hydration-product structure characterised by nano-indentation. They reported that the dependence of interlayer bond strength on rheology is not simply monotonic. In their principal dataset, relative bond strength decreased from 204.9% to 76.4% as the initial static yield stress of the printing mixture rose from 2.2 to 943.6 Pa, driven by increasing macro-interfacial porosity.

In a separate experiment designed to compare the effect of two different admixture strategies on yield stress and bond strength [26], when silica fume content was raised from 0% to 16% while superplasticiser dosage was adjusted to hold yield stress approximately constant (186.3 ± 33.4 Pa), relative bond strength increased from 69.7% to 112.3%. When yield stress was instead raised further, from 186.3 to 1260.9 Pa, via increased superplasticiser dosage while silica fume content also rose, bond strength fell sharply to 32.3% of the reference value, an effect the authors attributed to a competitive synergy between admixture-driven densification of the hydration products and workability loss, in which the latter dominates once yield stress increases substantially. Şahin and Mardani [32], synthesising this and other rheology-focused studies, further concluded that reduced surface moisture, rather than increased thixotropy per se, is the more consistent correlate of reduced bond strength across the broader literature reviewed, corroborating, from a substantially different set of primary sources, the surface-moisture-centred interpretation already advanced for Mechanism A via Moelich et al. [12] and Roussel [21].

Ding et al. [14] reviewed the existing analytical and numerical models for interlayer microstructure and mechanical properties and explicitly compared analytical modelling approaches for 3DCP interfaces, providing, to the authors' knowledge, the closest existing precedent to the model-comparison exercise undertaken in the present work, though without organising that comparison around an explicit mechanism taxonomy.

The stress–strain response of 3DCP concrete under tensile stresses parallel to the printing layers, and under compression in either direction, is qualitatively analogous to conventionally cast concrete [3]. Within the present taxonomy, this is the clearest macroscopic signature that Mechanism B is substantially mobilised under these loading conditions, in contrast to its near-total absence under tensile stresses perpendicular to the layers (normal to interfaces).

4.3. Literature Relevant to Mechanism C (Friction)

Friction is, by comparison with Mechanisms A, B, and D, markedly under-represented as an object of direct experimental study in the 3DCP interlayer literature reviewed for this work. No study identified in the present review isolates frictional resistance at the interlayer

interface independently of adhesive and cohesive contributions, in the way that, for example, a shear-friction test with controlled applied normal precompression across a fully degraded interface would. The closest indirect evidence comes from two sources external to the interlayer-adhesion literature proper: Kruger et al. [33] reported a shape-retention model for fresh 3DCP material based on a Mohr–Coulomb-type yield criterion, applied to the fresh, unbonded state of the material rather than to a hardened interlayer interface, and which does not address deposition onto preceding filament layers, and the work [17] on masonry interfaces, in which a Mohr–Coulomb friction law, calibrated experimentally for a discrete brick–mortar interface after cohesive resistance is exhausted, provided the residual-strength branch of the traction–separation law used in numerical validation. We regard this absence of direct evidence for Mechanism C in the hardened 3DCP interlayer literature as a genuine gap, distinct from (and in our reading more severe than) the terminological gaps identified in Section 1.

4.4. Literature Dominated by Mechanism D (Mechanical Interlocking)

A well-defined strand of the literature investigates geometric modification of the printed surface as a strategy to improve interlayer strength, and is here interpreted as probing Mechanism D. Zareiyan and Khoshnevis [27] reported a 26% strength improvement specifically in splitting tests (17% in direct compression along the layer interface) from a tongue-and-groove interlocking geometry, formed between mould-cast layers in a process simulating Contour Crafting deposition rather than by a grooved nozzle, but mechanically equivalent for the purpose of the present taxonomy. Their results are also the clearest existing demonstration that the geometric contribution of Mechanism D is non-monotonic with tongue depth (Figure 4b): strength increased for tongue depths up to 0.5″, but a further increase to 0.75″ returned strength to the same level as the unmodified base case, indicating that beyond an optimal geometry the interlocking contribution can be lost entirely rather than merely plateauing. He et al. [28] developed the most mechanistically explicit formulation, an analytical tooth-like interface model expressed in terms of tooth angle, void ratio, and an adhesion-to-cohesion ratio, reporting improvements of 291–294% in tension and 89% in shear for the geometries tested; these values refer to the geometries and baseline of that study and are not directly comparable with the changes reported in Sections 4.1 and 4.2. Marchment and Sanjayan [34–36] reported a "glue paste" strategy that increases the effective bond area between layers, with an improvement in bond strength of up to 60% under their test conditions. An increase in contact area is not, by itself, evidence of mechanical interlocking: a larger area of intimate contact enlarges the surface over which adhesion acts without necessarily introducing geometric interpenetration. The strategy is therefore assigned here to Mechanism A, and cited as a contrasting case that illustrates the distinction from the geometry-governed Mechanism D. Wang et al. [37] reported filament interlocking characterised via Brazilian-disc testing, digital image correlation, and acoustic emission. To et al. [38] examined four (I/T/S/V-shaped) alternatives of interlocking configurations by finite-element analysis in LS-DYNA and experimental validation of the improvement of mechanical interlocking.

Kloft et al. [31], as was described in Section 3.4, provide a complementary process-level perspective; they reported markedly higher interfacial roughness in sprayed specimens, together with a lower interfacial air-void content than in extruded specimens. Unlike the deliberately engineered geometries discussed above, this roughness arises as an incidental consequence of the deposition method's kinetic energy rather than of a designed relief, illustrating that the magnitude of mechanism D can be modulated by process selection as well as by geometric design (Table 1). The same study also reported that the deposition time interval had no significant effect on flexural or compressive strength when the tested

interface was aligned perpendicular to the applied load, but a pronounced effect when aligned parallel to it, indicating a loading-orientation dependence.

4.5. Process-Variable-to-Mechanism Mapping

Table 1 synthesises the mapping between manufacturing/process variables reported across the reviewed literature and the proposed mechanisms of Section 3 that each variable is here interpreted as primarily modulating. Variables are classified as primary where the reviewed literature provides direct evidence of a dominant effect on a single mechanism, and secondary where evidence suggests a modulating but non-dominant effect on an additional mechanism. We consider that this table makes explicit an assignment that is currently distributed implicitly across several individually framed experimental studies.

Table 2 shows the experimental conditions, as reported by the original authors, of the studies whose quantitative results are cited in Sections 3.4 and 4.

A further consequence of organising the literature by mechanism rather than by process variable is that it becomes possible to ask, for each experimental test method commonly used in this field, which mechanism(s) it actually isolates. Splitting tests and direct tensile tests applied perpendicular to the layers (e.g., [2,4,5]) predominantly probe Mechanism A under low or zero normal compression, with a possible contribution from B depending on curing time. Shear tests conducted without controlled normal precompression (e.g., [6,7]) necessarily convolve Mechanisms A, B, and a normal-stress component that is not the intended loading direction. Fracture-mechanics-based tests employing pre-notched specimens and energy-release-rate criteria [8] are, in our reading, the methodologically closest existing approach to isolating a well-defined mechanical event (crack penetration versus deflection at the interface), but remain framed in terms of a critical energy ratio rather than in terms of the mechanism taxonomy proposed here. No test method identified in the present review was designed explicitly to isolate Mechanism C from Mechanism D in a geometrically interlocked interface, which we identify, together with the general under-representation of Mechanism C, as a methodological gap to be addressed.

Loading orientation relative to the interface plane is itself a further, often implicit, methodological variable. According to [31], increased deposition time interval degraded flexural and compressive strength only when the interface was loaded parallel to it, with no measurable effect under perpendicular loading, indicating that a given process variable's apparent influence on "bond strength" can depend as much on the test's loading direction as on the mechanism it is presumed to isolate.

5. Confronting the Proposed Taxonomy Against Existing Constitutive Evidence

This work introduces Mechanisms A–D as a conceptual organisation; the present section tests whether that organisation has explanatory power against constitutive evidence that already exists. A taxonomy that cannot be confronted against existing data would be, at best, a restatement of terminology; the purpose of this section is to show that it is not.

The model developed in [3] for 3DCP concrete under uniaxial loading provides the most direct available test of the taxonomy's central claim: that the direction of loading relative to the printing layers determines which mechanisms are mobilised, and that this determination is visible in the macroscopic stress–strain response, subject to the mechanistic interpretation developed below. Under compression, in either direction relative to the layers, and under tensile stresses parallel to the layers, the stress–strain diagram remains qualitatively analogous to that of conventionally cast concrete with the same functional form, differing in the magnitude of peak stress and in the corresponding strain. Within the present taxonomy, this is the expected signature of a regime in which Mechanism B

(cohesion) is substantially mobilised: sufficient material continuity exists across the ITR for the bonded material to develop and sustain post-elastic deformation before failure, exactly as the bulk cast material does. Under tensile stresses perpendicular to the printing layers, by contrast, there is a qualitatively different response: the stress–strain relationship is closely approximated by a straight ascending line from the onset of loading to failure, with the failure limit corresponding to the adhesive strength R_{adh}, and with brittle failure characterised by an unloading slope approaching zero ($\alpha \approx 0$). Within the present taxonomy, this response is consistent with a regime in which Mechanism A (adhesion) governs, with substantial cohesion-related resistance (Mechanism B) not mobilised before the adhesive bond (the weakest link in this loading direction) fails first (Figure 3).

The adhesion/cohesion asymmetry reported in [3] is consistent with the fracture-mechanics analysis of Subramaniam et al. [8], who studied notched 3DCP beams by linear elastic fracture mechanics and digital image correlation. They show that a crack impinging on an interlayer interface deflects along it, instead of penetrating the next layer, when the critical energy release rate of the interface (G_{intc}) falls below about 1/3.74 of that for penetration (G_{mc}), that is, when G_{mc}/G_{intc} exceeds 3.74. The threshold was obtained from a finite-element analysis of their beam geometry and is close to the value given by He [28] for similar materials; G_{intc} was not measured directly, and the deflection observed at the 9 and 20 min interfaces is interpreted as a fall of G_{intc} below that threshold. This is a criterion for crack-path selection that contrasts an interface resistance (G_{intc}) with that of the layer material (G_{mc}), and we read it as consistent with the distinction between Mechanism A and Mechanism B. The two results, however, were obtained for different quantities (stress–strain response in [3]; crack path in [8]) and with different methods and frameworks, and they do not by themselves establish the physical reality of the proposed partition. The comparison also shows that R_{adh}, as defined and measured in [3], is a measured strength of the interface under tension perpendicular to the layers, rather than a curve-fit constant. Within the present taxonomy, that configuration and the notched fracture configuration of [8] can be regarded as tests in which Mechanism A is expected to govern the response, a reading that is ours and was not made in the original publications.

It is important to note that the study on brick–mortar contact stiffness [17] is invoked in the present paper strictly as a methodological precedent, not as a claim of material equivalence between masonry joints and 3DCP interlayer interfaces. The two systems differ in essential respects: a masonry joint is formed between two chemically and mechanically distinct materials placed in a single, near-simultaneous construction event, whereas a 3DCP interlayer interface is formed between two instances of the same material system separated by a finite, process-controlled time interval, precisely the distinction that motivates the ITR concept. The two systems should not, on this basis, be expected to share calibrated parameter values. What the two systems do share is the general mathematical structure required to represent a discrete, cohesive–frictional interface: a traction-separation law, a damage variable governing degradation from peak to residual capacity, and the empirical demonstration that coupling between normal and tangential stress components can develop even under nominally single-direction loading (Figure 6).

The measurement reported in [17] was obtained using a full-field, physically instrumented experimental-numerical procedure, not inferred indirectly. So, we regard this as directly relevant evidence that a similar coupling should be actively tested for, rather than assumed negligible, in any future experimental or numerical characterisation of 3DCP interlayer interfaces under combined or nominally pure shear loading.

Of the 38 sources in the corpus, six formulations were selected for this comparison. A formulation was included if it (i) provides an explicit analytical, constitutive or cohesive-zone representation specific to the response of 3DCP interlayers, and (ii) discloses enough

information to identify the physical or phenomenological quantities associated with one or more of the proposed mechanisms. These formulations are therefore those meeting the criteria within the corpus of Section Literature Search Strategy and Scope, not a census of published models, and the conclusions below are restricted to them and to what each paper reports. Table 3 indicates, for each formulation, which mechanisms are represented explicitly through an identifiable parameter and which are not represented and are therefore neglected or subsumed into another term. Here, "not represented" and "not explicitly separated" mean that no explicit term was identified in the formulation as published, not that the corresponding physical contribution is absent.

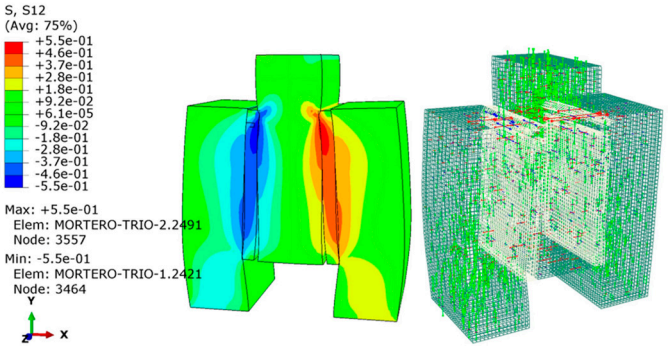


Figure 6. Induced normal stress at a brick–mortar interface under nominally pure shear loading, demonstrating normal–tangential coupling in a discrete cementitious interface analogous to the 3DCP (Source: [17]).

Table 3. Confrontation of existing 3DCP interface formulations against Mechanisms A–D.

Formulation	Mechanism				Neglected/Subsumed
	A (Adhesion)	B (Cohesion)	C (Friction)	D (Interlocking)	
Kabantsev [3]: Orthotropic σ–ε model.	Explicit (R_{adh}, tensile strength perpendicular to layers)	Explicit (tension parallel to layers/compression branch)	Not represented	Not represented	C, D absorbed implicitly into direction-dependent constants.
van den Heever [19]: Cohesive Zone Method (CZM).	Represented via cohesive strength parameter	Represented via cohesive stiffness/fracture energy	Not explicitly separated	Not explicitly separated	C, D not distinguished from cohesive parameters.
Geng et al. [26]: Dual hierarchical model, $\sigma = K(1-P)\sqrt{E}$	Not explicitly separated	Explicit (porosity P, modulus E)	Not represented	Not represented	A was subsumed into porosity term; C, D absent.
He et al. [28]: Tooth-like interface model.	Explicit (adhesion-to-cohesion ratio term)	Explicit (same ratio term, denominator)	Not explicitly separated from D	Explicit (tooth angle, void ratio)	C not separated from D's geometric contribution
An et al. [20]: Tension-compression anisotropic cohesive model.	Represented via direction-dependent cohesive strength	Represented via direction-dependent cohesive stiffness	Not explicitly separated	Not represented as an independent term	C, D absorbed into anisotropic cohesive parameters.
Moelich et al. [12]: Moisture-based analytical model	Explicit (surface-moisture-driven)	Not represented	Not represented	Not represented	B, C, D outside model scope by design.

Two observations follow from Table 3 that are material to the argument of the present paper: First, none of the six formulations examined represents all four mechanisms as independently identifiable parameters (constitutive contributions). Each formulation is internally consistent and empirically validated within the scope for which it was developed, but each achieves that consistency by explicitly representing between one and three

mechanisms while allowing the remainder contributions to be implicitly absorbed into the calibrated value of another parameter. This is not, in our reading, a flaw in any individual study; it is the expected consequence of the absence, prior to the present work, of an explicit taxonomy against which a formulation's scope could be checked. Second, an explicit normal-stress-dependent frictional contribution (Mechanism C) is the mechanism most consistently absent across all six formulations examined, consistent with the gap identified independently from the experimental literature. Where a formulation does allow for post-peak residual capacity (the CZM approach of [19], and implicitly the cohesive-damage framework of [20]), that residual capacity is represented through the same damage-degradation formalism used for the peak response, rather than through an explicitly frictional term dependent on normal stress. The distinction is important because a model may reproduce part of the macroscopic response without allowing the frictional component to be separately quantified or transferred to a different loading condition.

6. Requirements for a Future Constitutive Treatment of 3DCP Interlayer Interfaces

The proposal of a fully calibrated constitutive law would require dedicated experimental and numerical work beyond the scope of this paper. What the synthesis of Sections 3–5 does allow is the formulation of an explicit, falsifiable set of requirements that any such future constitutive law should satisfy in order to be consistent with the physical and mechanical evidence assembled here. We present these as a numbered list (R1–R5), so that each requirement can be checked independently against a future formulation.

- R1: *Explicit, separable representation of friction*. Table 3 shows that none of the six examined formulations for 3DCP interlayer interfaces represents Mechanism C as an independently identifiable, normal-stress-dependent term. A future formulation should include an explicit frictional contribution separable from the cohesive/adhesive damage formalism governing peak response, so that residual post-peak capacity is not implicitly attributed to incomplete cohesive damage alone.
- R2: *Direction-dependent mobilisation of adhesion and cohesion, rather than reliance on a single scalar bond parameter*. The directional behaviour discussed in Section 3.2 suggests that the relative contribution of adhesion- and cohesion-related resistance may depend on the orientation of loading with respect to the printing direction. Kabantsev's model [3] provides a relevant phenomenological representation of directional asymmetry through different branches and parameters. However, the correspondence between these branches and individual microscopic mechanisms should not be regarded as experimentally established solely from the macroscopic stress–strain response. A future constitutive formulation should therefore preserve the possibility of direction-dependent response while explicitly stating which parameters represent measurable mechanisms, which are phenomenological, and which combine several physical contributions. A single isotropic bond-strength parameter may be insufficient for applications requiring directional resolution, but its adequacy should be assessed against the loading regime, the required prediction accuracy, and the available experimental evidence.
- R3: *Normal–tangential coupling treated as an open empirical question, not a modelling convenience*. The coupled-stress evidence, obtained for an analogous discrete interface [17], indicates that decoupling the normal and tangential response of a bonded cementitious interface (the common simplification in cohesive-zone formulations, including several of those reviewed in Table 3) is a modelling choice requiring explicit justification for 3DCP interlayer interfaces specifically, rather than a default assumption. A future formulation should either (i) include coupling terms explicitly, or (ii) report the specific evidence justifying their omission for the loading regime and geometry considered.

This requirement is precautionary rather than evidentiary for 3DCP specifically, since the coupling evidence available at present derives from an analogous discrete-interface system rather than from 3DCP interlayer testing.

- R4: *Explicit homogenisation step for geometrically engineered interlocking*. Where the manufacturing process includes deliberate geometric relief (grooved/ribbed nozzles or other devices), a future formulation should state explicitly how the finite ITR-scale geometry (tooth angle, pitch, depth, etc.) is homogenised into the equivalent traction–separation response assigned to the idealised interface, following the precedent already set analytically by He et al. [28], rather than absorbing the geometric effect into an unspecified increase in an otherwise geometry-agnostic bond-strength parameter, as several of the formulations in Table 3 implicitly do.
- R5: *Parameters interpretable in terms of the physical state of the ITR*. Where feasible, calibrated parameters should be traceable to a measurable physical state of the ITR at the time of loading (surface moisture, interfacial porosity, degree of hydration) rather than functioning solely as curve-fit constants against a process-scheduling variable such as elapsed time. Moelich et al.'s [12] moisture-based model and Geng et al.'s [26] porosity-based model are cited in this work as existing precedents for this requirement, each covering one mechanism; a future formulation aiming to represent multiple mechanisms simultaneously should preserve this property for each.

We emphasise that R1–R5 are requirements derived from the synthesis in Sections 3–5, not requirements imposed a priori; each is traceable to a specific gap or a specific piece of confronting evidence discussed above. A future constitutive proposal satisfying R1–R5 would address the specific conceptual and modelling gaps identified in this synthesis. Whether such a formulation constitutes an improvement over existing models would nevertheless require independent assessment through calibration, validation, comparison of predictive performance, and evaluation of numerical robustness. Several of the requirements (R2, R5 in particular) are already partially satisfied by existing single-mechanism formulations and require integration rather than invention.

To make future experimental evidence comparable, and so that interlayer results can be interpreted in terms of the mechanisms proposed here, studies should report as a minimum: mixture proportions; interlayer interval and environmental conditions (temperature, relative humidity, evaporation or surface moisture); curing regime and testing age; loading mode and interface orientation; number of replicate specimens and their dispersion; the reference condition and normalisation used; and the failure location (along the contact plane (interface) or into the layer interior).

7. Conclusions

The present work is conceptual and synthetic in nature; it does not report new experimental data nor propose a calibrated constitutive law, by deliberate scope decision rather than omission. This paper has proposed a conceptual and mechanistic framework for interlayer stress transfer in extrusion-based 3D printed concrete, developed in four steps.

First, it introduced the Interface Transition Region (ITR), which represents the finite material region generated by the contact between two cementitious surfaces of the same material system but with different physicochemical histories at the instant of deposition, as deliberately distinct from the classical Interfacial Transition Zone (ITZ) of conventional concrete, and established the complementary physical/mechanical levels of description required to relate the ITR to the idealised, zero-thickness interface used in structural-scale modelling.

Second, it proposed a taxonomy of four stress-transfer mechanisms: adhesion (A), cohesion (B), friction (C), and mechanical interlocking (D), each with a distinguishable physical origin, dependence on process parameters, and constitutive signature, organised

across four interaction levels (formation, transfer, damage, residual). Mechanical interlocking was shown to require the two-level description as a physical necessity, not a convenience, since engineered geometric relief cannot be represented directly at a zero-thickness surface without an explicit homogenisation step.

Third, the taxonomy was examined against selected experimental, analytical, and numerical evidence rather than being presented solely as an abstract classification. The comparison suggests that the directional response described by the orthotropic model for 3DCP concrete may be interpreted in terms of different relative contributions of adhesion- and cohesion-related resistance; however, this correspondence remains a mechanistic interpretation rather than a direct experimental separation of the mechanisms. The evidence concerning coupled normal–tangential stress transfer is invoked as a methodological analogy rather than as direct material evidence for 3DCP interlayer interfaces. The comparison of six constitutive and analytical formulations did not identify a model that represents all four mechanisms as independently identifiable contributions. In the formulations examined, an explicit normal-stress-dependent frictional contribution was also not identified. This result indicates a potential modelling gap, but it should not be interpreted as proof that frictional effects are entirely absent from all existing formulations or from the physical response of 3DCP interfaces. Further experimental work specifically designed to isolate contact-related resistance would be required to assess the magnitude and constitutive role of friction.

Fourth, this synthesis was translated into five explicit, falsifiable requirements (R1–R5) that a future constitutive treatment of 3DCP interlayer interfaces should satisfy, ranging from the explicit, separable representation of friction to the physical interpretability of calibrated parameters in terms of the ITR's measurable state. These requirements, together with the shared methodological foundation for the traction–separation formulation, scalar damage representation, and finite-element implementation with explicit mesh-sensitivity verification, define a direct path toward the constitutive and numerical development planned as subsequent stages of this research programme, targeting a physically interpretable, direction-dependent, and numerically robust representation of the 3DCP interlayer interface suitable for structural-scale analysis.

Author Contributions: Conceptualization, D.C.-Z.; methodology, D.C.-Z.; validation, O.V.K.; formal analysis, D.C.-Z.; investigation, D.C.-Z., O.V.K. and A.V.K.; resources, D.C.-Z., O.V.K. and A.V.K.; data curation, D.C.-Z.; writing—original draft preparation, D.C.-Z.; writing—review and editing, D.C.-Z., O.V.K. and A.V.K.; visualization, D.C.-Z.; final review, O.V.K.; funding acquisition, O.V.K. and A.V.K. All authors have read and agreed to the published version of the manuscript.

Funding: This work was carried out as part of the implementation of the Development Programme of the Federal State Budgetary Educational Institution of Higher Education "National Research Moscow State University of Civil Engineering" for 2025–2036. The Article Processing Charge (APC) was funded by the National Research Moscow State University of Civil Engineering.

Data Availability Statement: The original contributions presented in the study are included in the article. Further inquiries can be directed to the corresponding author.

Conflicts of Interest: The authors declare no conflicts of interest. The funders had no role in the design of the study; in the collection, analysis, or interpretation of data; in the writing of the manuscript; or in the decision to publish the results.

Appendix A.

Table A1 lists the 38 sources that form the corpus of this paper with the type of study, the evidence domain and the mechanism assigned in this work. This assignment is an interpretation by the authors of the present paper, not a finding of the original studies, except where the last column states it.

Table A1. Corpus of 38 sources, with the mechanism assigned in this work and the basis of that assignment.

Ref.	Study	Type of Study	Evidence Domain	Mechanism	Process Variable	Basis of Assignment
[1]	Buswell et al., 2018	Research roadmap	Review or roadmap	—	Research framework	Not assigned
[2]	Le et al., 2012	Experimental	Interlayer	A/—	Interlayer interval (0 min–7 d)	Inferred
[3]	Kabantsev, 2024	Experimental + model	Interlayer	A/B	Loading direction	Inferred
[4]	Wolfs et al., 2019	Experimental	Interlayer	A/—	Interval + drying	Inferred
[5]	Skibicki et al., 2024	Experimental + FEM	Interlayer	A/B	Interval + micro-CT porosity	Inferred
[6]	Napolitano et al., 2020	Experimental	Interlayer	A/—	Interval (100–1800 s)	Inferred
[7]	Tay et al., 2018	Experimental	Interlayer	A/—	Interval (1–20 min)	Inferred
[8]	Subramaniam et al., 2024	Experimental + LEFM	Interlayer	A/—	Interval + fracture path	Inferred
[9]	Pan et al., 2022	Experimental + CFD	Interlayer	A/— (formation-level)	Nozzle stand-off + speed	Inferred
[10]	Weng et al., 2021	Experimental	Interlayer	A/—	Superplasticiser + thixotropy	Inferred
[11]	Zareiyan & Khoshnevis, 2018	Experimental	Interlayer	A/B	Mixture ingredients	Inferred
[12]	Moelich et al., 2021	Experimental + analytical model	Interlayer	A/—	Surface moisture	Declared
[13]	Babafemi et al., 2021	Review	Review or roadmap	—	(review)	Not assigned
[14]	Ding et al., 2023	Review	Review or roadmap	—	Microstructure	Not assigned
[15]	Mohan et al., 2021	Review	Review or roadmap	—	Material perspective	Not assigned
[16]	Liu et al., 2026	Review	Review or roadmap	—	Wall structures	Not assigned
[17]	Cajamarca-Zuniga & Kabantsev, 2026	Experimental + numerical	Analogous interface	C/—	Shear + induced normal stress	Inferred
[18]	Hillerborg et al., 1976	Analytical	Theoretical background	—/—	LEFM framework	Not assigned
[19]	van den Heever et al., 2020	Experimental + CZM	Interlayer	A/B	DTT + IST	Inferred
[20]	An et al., 2025	Numerical + experimental	Interlayer	A/B	Anisotropic cohesive model	Inferred
[21]	Roussel, 2018	Conceptual	Interpretive synthesis	A/—	Rheology + drying	Inferred
[22]	Wang, 2013	Numerical (RBSM)	Theoretical background	—	Meso-scale framework	Not assigned
[23]	Scrivener et al., 2004	Experimental (SEM)	Theoretical background	—	ITZ characterisation	Not assigned
[24]	Nerella et al., 2019	Experimental + SEM	Interlayer	A/B	Composition + interval	Inferred
[25]	Zhang et al., 2023	Experimental	Interlayer	A/—	Number of stacked layers	Inferred
[26]	Geng et al., 2020	Experimental + model	Interlayer	B/A	Porosity + elastic modulus	Inferred
[27]	Zareiyan & Khoshnevis, 2017	Experimental	Interlayer	D/—	Tongue-and-groove geometry	Inferred
[28]	He et al., 2022	Experimental + analytical model	Interlayer	D/A	Tooth angle + void ratio	Inferred
[29]	Rahul et al., 2019	Experimental	Interlayer	B/—	Porosity + bond shear	Inferred
[30]	Kabantsev & Cajamarca-Zuniga, 2023	Experimental	Analogous interface	— (C and D not isolated)	Unmodified brick vs. modified brick (interlocking)	Not assigned
[31]	Kloft et al., 2020	Experimental + CT	Interlayer	D/A	Shotcrete (SC3DP) vs. extrusion	Inferred
[32]	Şahin & Mardani, 2024	Review	Review or roadmap	—	Rheology + moisture	Not assigned
[33]	Kruger et al., 2020	Analytical + FEA	Bulk fresh material (no interlayer)	—	Shape retention	Not assigned
[34]	Marchment et al., 2019 (book)	Book chapter	Interlayer	A/—	Paste + interval	Inferred
[35]	Marchment & Sanjayan, 2019	Experimental	Interlayer	A/—	Paste interlayer	Inferred
[36]	Marchment et al., 2019 (M&D)	Experimental	Interlayer	A/—	Effective bond area	Inferred
[37]	Wang et al., 2026	Experimental	Interlayer	D/—	Filament interlocking	Inferred
[38]	To et al., 2024	Experimental + FEM	Interlayer	D/C	Interlocking I/T/S/V	Inferred

A = adhesion; B = cohesion; C = friction; D = mechanical interlocking. "Inferred": mechanism inferred by the authors of the present paper from the variable studied or measured; "Declared": mechanism named by the original authors; "Not assigned": no mechanism is assigned (reviews, theoretical background, bulk-material studies, or studies in which the contributions could not be separated).

References

1. Buswell, R.A.; Leal de Silva, W.R.; Jones, S.Z.; Dirrenberger, J. 3D Printing Using Concrete Extrusion: A Roadmap for Research. *Cem. Concr. Res.* **2018**, *112*, 37–49. [CrossRef]
2. Le, T.T.; Austin, S.A.; Lim, S.; Buswell, R.A.; Law, R.; Gibb, A.G.F.; Thorpe, T. Hardened Properties of High-Performance Printing Concrete. *Cem. Concr. Res.* **2012**, *42*, 558–566. [CrossRef]
3. Kabantsev, O. Adaptation of Concrete Model to 3D Printing Technology. *Buildings* **2024**, *14*, 3806. [CrossRef]
4. Wolfs, R.J.M.; Bos, F.P.; Salet, T.A.M. Hardened Properties of 3D Printed Concrete: The Influence of Process Parameters on Interlayer Adhesion. *Cem. Concr. Res.* **2019**, *119*, 132–140. [CrossRef]
5. Skibicki, S.; Szewczyk, P.; Majewska, J.; Sibera, D.; Ekiert, E.; Chung, S.-Y.; Sikora, P. The Effect of Interlayer Adhesion on Stress Distribution in 3D Printed Beam Elements. *J. Build. Eng.* **2024**, *87*, 109093. [CrossRef]
6. Napolitano, R.; Menna, C.; Asprone, D.; Del Giudice, L. Mechanical Characterization of Layer-by-Layer Interface in Concrete Elements Obtained by Additive Manufacturing. In *Proceedings of the Second RILEM International Conference on Concrete and Digital Fabrication*; Bos, F.P., Lucas, S.S., Wolfs, R.J.M., Salet, T.A.M., Eds.; Springer International Publishing: Cham, Switzerland, 2020; pp. 468–477.
7. Tay, D.Y.W.; Ting, A.G.H.; Panda, B.; He, L.; Tan, M.J. Bond Strength of 3D Printed Concrete. In *Proceedings of the 3rd International Conference on Progress in Additive Manufacturing*; Chua, C.K., Yeong, W.Y., Tan, M.J., Liu, E., Tor, S.B., Eds.; Nanyang Technological University: Singapore, 2018; p. 6.
8. Subramaniam, K.V.L.; Paritala, S.; Kulkarni, O.; Thakur, M.S. Fracture in 3D-Printed Concrete Beams: Deflection and Penetration of Impinging Cracks at Layer Interfaces. *J. Eng. Mech.* **2024**, *150*, 4024093. [CrossRef]
9. Pan, T.; Guo, R.; Jiang, Y.; Ji, X. How Do the Contact Surface Forces Affect the Interlayer Bond Strength of 3D Printed Mortar? *Cem. Concr. Compos.* **2022**, *133*, 104675. [CrossRef]
10. Weng, Y.; Li, M.; Zhang, D.; Jen, M.; Qian, S. Investigation of Interlayer Adhesion of 3D Printable Cementitious Material from the Aspect of Printing Process. *Cem. Concr. Res.* **2021**, *143*, 106386. [CrossRef]
11. Zareiyan, B.; Khoshnevis, B. Effects of Mixture Ingredients on Interlayer Adhesion of Concrete in Contour Crafting. *Rapid Prototyp. J.* **2018**, *24*, 584–592. [CrossRef]
12. Moelich, G.M.; Kruger, J.; Combrinck, R. Modelling the Interlayer Bond Strength of 3D Printed Concrete with Surface Moisture. *Cem. Concr. Res.* **2021**, *150*, 106559. [CrossRef]
13. Babafemi, A.J.; Kolawole, J.T.; Miah, M.J.; Paul, S.C.; Panda, B. A Concise Review on Interlayer Bond Strength in 3D Concrete Printing. *Sustainability* **2021**, *13*, 7137. [CrossRef]
14. Ding, T.; Xiao, J.; Mechtcherine, V. Microstructure and Mechanical Properties of Interlayer Regions in Extrusion-Based 3D Printed Concrete: A Critical Review. *Cem. Concr. Compos.* **2023**, *141*, 105154. [CrossRef]
15. Mohan, M.K.; Rahul, A.V.; Van Tittelboom, K.; Schutter, G. De Extrusion-Based Concrete 3D Printing from a Material Perspective: A State-of-the-Art Review. *Cem. Concr. Compos.* **2021**, *115*, 103855. [CrossRef]
16. Liu, B.; Agusril, S.; Woen, E.L.; Khai, W.J.; Xiang, P. Advanced Strategies for Comfort and Mechanical Performance of 3D-Printed Concrete Wall Structures: A State-of-the-Art Review. *Buildings* **2026**, *16*, 3515. [CrossRef]
17. Cajamarca-Zuniga, D.; Kabantsev, O. V Experimental Calibration and Numerical Validation of Brick–Mortar Contact Stiffness for Detailed Micromodelling of Masonry: Evidence of Induced Normal Stresses Under Shear. *Buildings* **2026**, *16*, 2905. [CrossRef]
18. Hillerborg, A.; Modeer, M.; Petersson, P.E. Analysis of Crack Formation and Crack Growth in Concrete by Means of Fracture Mechanics and Finite Elements. *Cem. Concr. Res.* **1976**, *6*, 773–782. [CrossRef]
19. van den Heever, M.; Bester, F.; Pourbehi, M.; Kruger, J.; Cho, S.; van Zijl, G. Characterizing the Fissility of 3D Concrete Printed Elements via the Cohesive Zone Method. In *Proceedings of the Second RILEM International Conference on Concrete and Digital Fabrication*; Bos, F.P., Lucas, S.S., Wolfs, R.J.M., Salet, T.A.M., Eds.; Springer International Publishing: Cham, Switzerland, 2020; pp. 489–499.
20. An, N.; Wang, H.; Wang, P.; Xu, C.; Liu, M. Tension-Compression Anisotropic Cohesion Model for the Interlayer Interface of 3D-Printed Concrete Compression Specimens. *J. Build. Eng.* **2025**, *107*, 112800. [CrossRef]
21. Roussel, N. Rheological Requirements for Printable Concretes. *Cem. Concr. Res.* **2018**, *112*, 76–85. [CrossRef]
22. Wang, L.C. Meso-Scale Numerical Modeling of the Mechanical Behavior of Reinforced Concrete Members. *Int. J. Eng. Technol.* **2013**, *5*, 680–684. [CrossRef]
23. Scrivener, K.L.; Crumbie, A.K.; Laugesen, P. The Interfacial Transition Zone (ITZ) Between Cement Paste and Aggregate in Concrete. *Interface Sci.* **2004**, *12*, 411–421. [CrossRef]
24. Nerella, V.N.; Hempel, S.; Mechtcherine, V. Effects of Layer-Interface Properties on Mechanical Performance of Concrete Elements Produced by Extrusion-Based 3D-Printing. *Constr. Build. Mater.* **2019**, *205*, 586–601. [CrossRef]
25. Zhang, Y.; Yang, L.; Qian, R.; Liu, G.; Zhang, Y.; Du, H. Interlayer Adhesion of 3D Printed Concrete: Influence of Layer Stacked Vertically. *Constr. Build. Mater.* **2023**, *399*, 132424. [CrossRef]

26. Geng, Z.; She, W.; Zuo, W.; Lyu, K.; Pan, H.; Zhang, Y.; Miao, C. Layer-Interface Properties in 3D Printed Concrete: Dual Hierarchical Structure and Micromechanical Characterization. *Cem. Concr. Res.* **2020**, *138*, 106220. [CrossRef]
27. Zareiyan, B.; Khoshnevis, B. Effects of Interlocking on Interlayer Adhesion and Strength of Structures in 3D Printing of Concrete. *Autom. Constr.* **2017**, *83*, 212–221. [CrossRef]
28. He, L.; Li, H.; Chow, W.T.; Zeng, B.; Qian, Y. Increasing the Interlayer Strength of 3D Printed Concrete with Tooth-like Interface: An Experimental and Theoretical Investigation. *Mater. Des.* **2022**, *223*, 111117. [CrossRef]
29. Rahul, A.V.; Santhanam, M.; Meena, H.; Ghani, Z. Mechanical Characterization of 3D Printable Concrete. *Constr. Build. Mater.* **2019**, *227*, 116710. [CrossRef]
30. Kabantsev, O.V.; Cajamarca-Zuniga, D. Proposal for Improving the Solid Clay Brick Contact Surface to Increase the Initial Shear Strength of Masonry. *Mater. Today Proc.* **2023**, *8*. [CrossRef]
31. Kloft, H.; Krauss, H.W.; Hack, N.; Herrmann, E.; Neudecker, S.; Varady, P.A.; Lowke, D. Influence of Process Parameters on the Interlayer Bond Strength of Concrete Elements Additive Manufactured by Shotcrete 3D Printing (SC3DP). *Cem. Concr. Res.* **2020**, *134*, 106078. [CrossRef]
32. Şahin, H.G.; Mardani, A. How Does Rheological Behaviour Affect the Interlayer-Bonding Strength of 3DPC Mixtures? *J. Adhes. Sci. Technol.* **2024**, *38*, 1353–1377. [CrossRef]
33. Kruger, J.; Zeranka, S.; van Zijl, G. A Rheology-Based Quasi-Static Shape Retention Model for Digitally Fabricated Concrete. *Constr. Build. Mater.* **2020**, *254*, 119241. [CrossRef]
34. Marchment, T.; Sanjayan, J.G.; Nematollahi, B.; Xia, M. Interlayer Strength of 3D Printed Concrete: Influencing Factors and Method of Enhancing. In *3D Concrete Printing Technology*; Sanjayan, J.G., Nazari, A., Nematollahi, B., Eds.; Butterworth-Heinemann: Oxford, UK, 2019; pp. 241–264. ISBN 978-0-12-815481-6.
35. Marchment, T.; Sanjayan, J. Method of Enhancing Interlayer Bond Strength in 3D Concrete Printing. In *Proceedings of the First RILEM International Conference on Concrete and Digital Fabrication—Digital Concrete 2018*; Wangler, T., Flatt, R.J., Eds.; Springer International Publishing: Cham, Switzerland, 2019; pp. 148–156.
36. Marchment, T.; Sanjayan, J.; Xia, M. Method of Enhancing Interlayer Bond Strength in Construction Scale 3D Printing with Mortar by Effective Bond Area Amplification. *Mater. Des.* **2019**, *169*, 107684. [CrossRef]
37. Wang, L.; Huang, Z.; Nguyen, G.D.; Karakus, M. Improving Interlayer Adhesion of 3D Printed Concrete by Filament Interlocking. *J. Build. Eng.* **2026**, *121*, 115700. [CrossRef]
38. To, Q.B.; Pham, K.V.A.; Lee, G.; Shin, M.; Shin, D.W.; Lee, K. Experimental and FEM Evaluation of the Influence of Interlayer Bonding Strength in 3D Printed Concrete Members under Compressive and Flexural Loadings. *J. Build. Eng.* **2024**, *94*, 109979. [CrossRef]

Disclaimer/Publisher's Note: The statements, opinions and data contained in all publications are solely those of the individual author(s) and contributor(s) and not of MDPI and/or the editor(s). MDPI and/or the editor(s) disclaim responsibility for any injury to people or property resulting from any ideas, methods, instructions or products referred to in the content.